molecules

MDPI

Article

Structures and Spectroscopic Properties of Polysulfide Radical Anions: A Theoretical Perspective

Tristram Chivers [1,*] and Richard T. Oakley [2,*]

[1] Department of Chemistry, University of Calgary, Calgary, AB T2N 1N4, Canada
[2] Department of Chemistry, University of Waterloo, Waterloo, ON N2L 3G1, Canada
* Correspondence: chivers@ucalgary.ca (T.C.); oakley@uwaterloo.ca (R.T.O.)

Abstract: The potential involvement of polysulfide radical anions $S_n^{\bullet-}$ is a recurring theme in discussions of the basic and applied chemistry of elemental sulfur. However, while the spectroscopic features for n = 2 and 3 are well-established, information on the structures and optical characteristics of the larger congeners (n = 4–8) is sparse. To aid identification of these ephemeral species we have performed PCM-corrected DFT calculations to establish the preferred geometries for $S_n^{\bullet-}$ (n = 4–8) in the polar media in which they are typically generated. TD-DFT calculations were then used to determine the number, nature and energies of the electronic excitations possible for these species. Numerical reliability of the approach was tested by comparison of the predicted and experimental excitation energies found for $S_2^{\bullet-}$ and $S_3^{\bullet-}$. The low-energy (near-IR) transitions found for the two acyclic isomers of $S_4^{\bullet-}$ (C_{2h} and C_{2v} symmetry) and for $S_5^{\bullet-}$ (C_s symmetry) can be understood by extension of the simple HMO π-only chain model that serves for $S_2^{\bullet-}$ and $S_3^{\bullet-}$. By contrast, the excitations predicted for the *quasi*-cyclic structures $S_n^{\bullet-}$ (n = 6–8) are better described in terms of $\sigma \rightarrow \sigma^*$ processes within a localized 2c-3e manifold.

Keywords: polysulfide chemistry; radical anions; structures; spectroscopic properties; time-dependent density functional theory

Citation: Chivers, T.; Oakley, R.T. Structures and Spectroscopic Properties of Polysulfide Radical Anions: A Theoretical Perspective. *Molecules* **2023**, *28*, 5654. https://doi.org/10.3390/molecules28155654

Academic Editor: Petr Kilián

Received: 20 June 2023
Revised: 17 July 2023
Accepted: 24 July 2023
Published: 26 July 2023

1. Introduction

Polysulfide radical anions $S_n^{\bullet-}$ (n = 2–8) play a pivotal role as intermediates in the sulfur ↔ sulfide redox cycle [1–4]. The influence of these short-lived species is frequently invoked in contemporary investigations of sulfur chemistry, including alkali-metal-sulfur batteries [5–7], organic syntheses [8], biological chemistry [9,10], geochemical processes involving metal transport [11–13] and quantum-dot sensitized solar cells [14,15]. In solution, polysulfide radical anions are readily oxidized by atmospheric oxygen, but the smaller members can be trapped in an aluminosilicate matrix and are known to be the chromophores in yellow ($S_2^{\bullet-}$), blue ($S_3^{\bullet-}$) and green (simultaneous presence of $S_2^{\bullet-}$ and $S_3^{\bullet-}$) ultramarines [16] and related sodalite-group minerals [17]. The diatomic $S_2^{\bullet-}$ and the triatomic $S_3^{\bullet-}$ (C_{2v}) radical anions are readily detected in solution or in the solid state by their characteristic UV-visible, Raman or EPR spectra [18]. Indeed, one or more of these techniques is commonly invoked to provide evidence for the role of $S_3^{\bullet-}$ as an in-situ generated reagent in organic synthesis [8].

In contrast to the well-established spectroscopic signatures of $S_2^{\bullet-}$ and $S_3^{\bullet-}$, evidence for the larger members of the family (n = 4–8) is fragmentary and often conflicting. Of these species, $S_4^{\bullet-}$ has a long but somewhat checkered history. In 1970, as part of his pioneering study on solutions of alkali-metal polysulfides in electron-pair donor solvents, e.g., DMF, HMPA, Seel attributed a visible absorption at ca. 515 nm to $S_4^{\bullet-}$ [19], but later the band was reassigned to a dimer [20], an example of which has recently been structurally characterized in a dinuclear Bi(III)Bi(III) complex [21]. In 1983 Clark et al. investigated the nature of the sulfur chromophore in ultramarine pink by Raman spectroscopy [22], but they

were unable to distinguish between S_4 and $S_4^{\bullet-}$ (or even S_3Cl). The association of a 490 nm band with $S_4^{\bullet-}$ has nonetheless persisted [9,23], and Chiba and co-workers have recently invoked formation of the radical anion during the photolysis of the closed-shell dianion S_4^{2-} [24–27]. The use of other techniques to identify $S_4^{\bullet-}$ in solution, notably Raman and IR spectroscopy [28–30], has been pursued, but band assignments based on calculated vibrational frequencies have been questioned [3]. Likewise, an EPR signal observed in solutions of lithium polysulfide solutions in DMF was proposed to belong to $S_4^{\bullet-}$ [31], but the isotropic *g*-value (2.031) lies close to that of the dominant radical anion $S_3^{\bullet-}$ (2.029) [32]. In principle, high field EPR spectroscopy could be used to distinguish between these (and other) polysulfide radical anions, and on this basis Chukanov et al. recently suggested the presence of $S_4^{\bullet-}$ in various sodalite minerals [33].

The larger anions $S_n^{\bullet-}$ (n = 5–8) are also acknowledged as potentially important intermediates in the $S_8 \leftrightarrow S^{2-}$ redox processes, as in the electrochemical reduction of cyclo-S_8, redox transformations in alkali metal-sulfur batteries [27] and the formation of polysulfides from photoexcited quantum dots [14,15]. Exploration of the stepwise electrochemical reduction of cyclo-S_8 in non-aqueous solvents has been extensively pursued, with formation of S_8^{2-} generally accepted by the battery community to occur first (Scheme 1) [3]. Initially, in 1970, Merritt and Sawyer claimed the preliminary formation of the one-electron reduction product $S_8^{\bullet-}$ [34], then revised this interpretation to a two-electron transfer [35], in agreement with the work of Bonnaterre and Cauquis [36] and also supported by results obtained by Hardacre and coworkers using ionic liquids as the solvent medium [37]. However, in 2008, the results of a detailed cyclic voltammetric study of the reduction of S_8 in various solvents were consistent with the formation of S_8^{2-} via two consecutive one-electron steps [38]. The potential for the involvement of $S_4^{\bullet-}$ in the S_8 reduction process has been argued [39–42], but in the absence of a clear spectroscopic signature for the anion, the issue has not been resolved. Although symmetrical dissociation of S_8^{2-} to give two $S_4^{\bullet-}$ radical anions is calculated to be exergonic [43], and an absorption band at ca. 700 nm was assigned to $S_4^{\bullet-}$ [44,45] in spectrochemical studies of the reduction of sulfur in DMSO and DMF, others insist that it has never been detected [46].

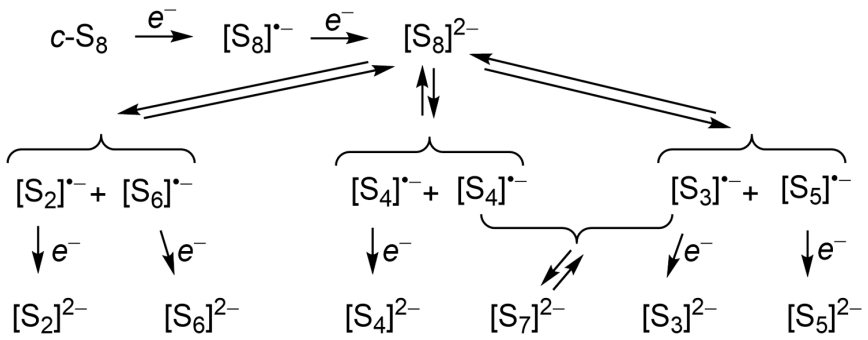

Scheme 1. Possible radical anion intermediates in the stepwise electrochemical reduction of *c*-S_8.

Surprisingly, although the preparation and structural characterization of several salts of the S_8^{2-} were reported more than 30 years ago [47,48], there is limited information on the behavior of ion-separated salts of S_8^{2-} in non-aqueous solvents. Formation of S_8^{2-} from S_8 has traditionally been interpreted to be followed by disproportionation to S_6^{2-} and $\frac{1}{4}S_8$ [39,43,49], the former dissociating to afford $S_3^{\bullet-}$ [48]. However, a disproportionation process simply represents a mass balance, and belies the reality that the formation of an eight-membered S_8 ring must involve the intermediacy of long chain polysulfide dianions S_n^{2-} with $n > 8$ and, possibly, polysulfide radical anions such as $S_n^{\bullet-}$ (n = 4, 6) [3]. Alternative fates for S_8^{2-} in dilute solution can be envisaged (Scheme 1) in terms of equilibria involving its symmetric and asymmetric dissociation to afford, in principle, the entire series of polysulfide radical anions $S_n^{\bullet-}$ (n = 2–6). Longer chain closed-shell dianions such as S_{10}^{2-} and S_{12}^{2-}, salts of which have recently been characterized [50,51], can then be viewed as arising from the reverse process, that is, symmetric coupling of the radical anions

$S_5^{\bullet-}$ and $S_6^{\bullet-}$, respectively, while association of $S_3^{\bullet-}$ and $S_4^{\bullet-}$ yields S_7^{2-}. Unfortunately, information on the electrochemical reduction of the cyclic allotropes S_6 and S_7 is lacking. That being said, in 2002 Dehnicke and coworkers isolated and structurally characterized crystals of the (orange/red) radical ion salt $[Ph_4P][S_6]$, the only such characterization of an ion-separated salt of a polysulfide radical anion [52]. The importance of this result is discussed below.

As demonstrated in this brief survey, there are many unsettled questions regarding the basic chemistry of elemental sulfur, in particular relating to the stability, structure and properties of radical ion products that may be generated during the sequential reduction of cyclo-S_8 or the oxidation of the sulfide ion S^{2-} [1]. These questions have given rise to ongoing controversies, many relating to the colors of these ephemeral species—what do they look like, and do they exist if they cannot be seen?

While the colors of $S_2^{\bullet-}$ and $S_3^{\bullet-}$ are well characterized, the optical properties of the larger *putative* polysulfide radical anions have been explored only to a very limited extent. Fabian et al. used density functional theory (DFT) methods to probe the excited states of $S_4^{\bullet-}$, and predicted a strong absorption in the near-IR region, with a weaker band near 350 nm for cis $S_4^{\bullet-}(C_{2v})$ isomer, which is slightly more stable than the trans (C_{2h}) isomer [53]. More recently, and using DFT and CASSCF methods, Rejmak confirmed that the cis $S_4^{\bullet-}$ radical anion could be identified by a strong absorption in the near-IR region [54] and proposed that the red chromophore in ultramarine red is *neutral* S_4 rather than the corresponding radical anion. Surprisingly, the excited state properties of the remaining radical ions in the series, that is $S_n^{\bullet-}$ (n = 5–8), have never been explored theoretically, perhaps because even their ground state geometries have remained somewhat of a puzzle.

The principal objective of the present article is to redress this issue, to fill in the blanks not only in regard to the spectroscopic signatures of these radical anions, that is, their excited state properties, but also to establish their ground state structures, particularly in solution in polar solvents, the media in which they are most likely to be generated.

2. Results

2.1. Structural Trends

In the following sections we describe the structural features and relative energies provided by spin unrestricted PBE0/D3/def2-QZVP calculations for the family of radical anions $S_n^{\bullet-}$ (n = 4–8). The results build upon the earlier systematic studies of Hunsicker et al. [55], Steudel [40] and Wong [56], but include several alternative shapes not previously considered. The possible effects of solvation are heavily stressed, as our overall aim has been to identify structures most likely to be present in solution in the polar solvents typically used for the spectroscopic observation of these species. To this end we performed not only standard "gas phase" geometry optimizations but also optimizations employing the polarized continuum model (PCM) to simulate solvation effects, with DMF (ε = 37.2) serving as a representative example. As observed by Steudel, the inclusion of solvation using the PCM approach leads to only minor geometrical adjustments, and for this reason only the "gas phase" structural parameters are presented in the main text (see Figure S1 for PCM-adjusted numbers). Solvation effects, however, have important energetic consequences, favoring structures with large molecular dipoles, and can play a pivotal role in adjusting the balance between structural alternatives which are otherwise closely matched energetically.

2.1.1. $S_2^{\bullet-}$ and $S_3^{\bullet-}$

Like molecular oxygen, the diatomic molecule S_2 possesses a triplet ground state [57]. Addition of an electron to one of the two half-filled π_g^* orbitals, to afford the $^2\Pi_g$ radical anion $S_2^{\bullet-}$, leads to an elongation of the S–S bond, calculated here = 1.996 Å. Attachment of a third sulfur introduces the possibility of structural options for $S_3^{\bullet-}$, namely linear ($D_{\infty h}$), equilateral and isosceles triangular (D_{3h} and C_{2v}, respectively); the last is established

as the energetically preferred. Structural parameters calculated here for the $^2B_1$ state, an S–S bond distance of 1.984 Å and inter-bond angle of 115.7°, are consistent with previous estimates [58,59].

2.1.2. $S_4^{\bullet-}$

Based on both experimental and theoretical evidence [48,49,60] the geometry of a discrete neutral S_4 molecule displays C_{2v} symmetry, consisting of a planar broken-ring structure with one "long" S–S bond, calculated here = 3.222 Å. The most appealing option for the corresponding $S_4^{\bullet-}$anion is also a planar C_{2v} structure (Figure 1a), akin to the neutral form but with the "long" S–S bond further stretched (calculated here = 3.505 Å). However, a C_{2h} isomer (Figure 1b), generated from the C_{2v} by a 180° rotation about the central S–S linkage, is also possible.

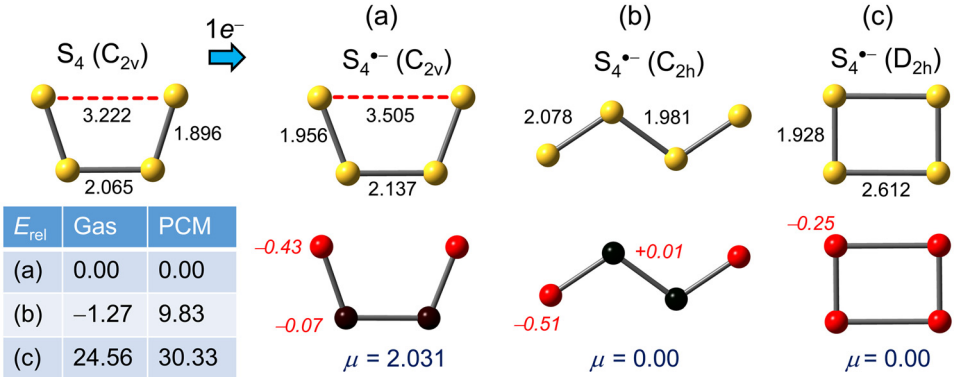

E_{rel}	Gas	PCM
(a)	0.00	0.00
(b)	−1.27	9.83
(c)	24.56	30.33

Figure 1. (U)PBE0/D3/def2-QZVP optimized geometries (distances in Å) for $S_4^{\bullet-}$, with Mulliken charges (in italics) and dipole moments μ (in Debye). Relative gas phase and PCM (=DMF) corrected total energies E_{rel} are in kJ mol^{-1}.

Frequency calculations confirm that both the C_{2v} (cis) and C_{2h} (trans) forms are true energetic minima, the latter being slightly more stable in the gas phase. But the energetic competition between the two ceases upon inclusion of PCM (=DMF) solvation, with the centrosymmetric (μ = 0) C_{2h} isomer rising relative to the C_{2v} form by nearly 10 kJ mol^{-1}. The presence of both isomers in solvents with a low dielectric constant may nonetheless be possible. Other structures, based on closed rings, have been explored by previous workers and found to be energetically much more high-lying. Re-examination here of these variants, none of which represents a true energetic minimum, indicates the centrosymmetric (μ = 0) D_{2h} modification (Figure 1c), formed by a Jahn–Teller distortion of a putative D_{4h} geometry [61], is the most stable of the closed-ring group, although it still lies well above the C_{2v} form and, with the inclusion of PCM, its relative energy rises even higher.

2.1.3. $S_5^{\bullet-}$

While the structure of neutral S_5 is unknown, an open envelope-like or chair shape with C_s symmetry has been predicted in previous studies [62,63], with the S–S bond bisected by the mirror plane slightly elongated. We concur with this result, and calculate the unique S–S distance = 2.157 Å. The apparent weakening may be attributed, in valence bond parlance, to lone-pair repulsion arising from the eclipsed alignment of the two neighboring S–S bonds. One-electron reduction to the radical anion $S_5^{\bullet-}$ leads to a variety of structural alternatives, the most obvious involving complete separation (to 4.095 Å) of the already weakened mirror-bisected linkage, to afford the distorted C_s chair illustrated in Figure 2a. Vibrational analysis confirms that the optimized structure represents a true energetic minimum and, as indicated by the associated Mulliken charge densities, negative charge is heavily localized on the two sulfurs associated with the "broken" bond. As expected, charge polarization, and its impact on the molecular dipole, increases with the inclusion of PCM (Table S1).

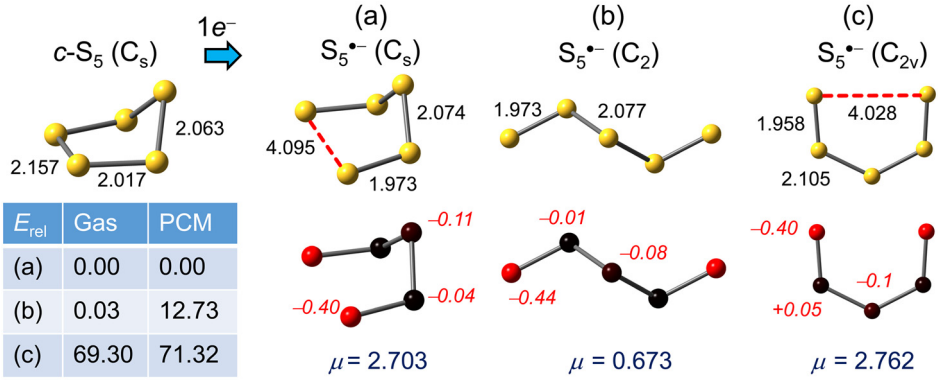

E_{rel}	Gas	PCM
(a)	0.00	0.00
(b)	0.03	12.73
(c)	69.30	71.32

Figure 2. (U)PBE0/D3/def2-QZVP optimized geometries (distances in Å) for $S_5^{\bullet-}$, with Mulliken charges (in italics) and dipole moments μ (in Debye). Relative gas phase and PCM (=DMF) corrected total energies E_{rel} are in kJ mol^{-1}.

Open-chain structures for $S_5^{\bullet-}$ are also possible; several variants have been explored by previous workers, but in our hands these all gravitate on optimization towards the twisted chain (C_2 symmetry) minimum shown in Figure 2b. It is almost co-energetic with the C_s chair, perhaps not surprisingly as the two structures are interconvertible by a 180° rotation of one of the terminal bonds. However, by virtue of the lower dipole moment of the open-chain form, a substantial gap opens with the inclusion of PCM. In addition, we have considered two "forced" planar modifications, one being the cis-cis C_{2v} geometry shown in Figure 2c. While it does not represent a stable minimum, and its relative energy is substantially higher than the related C_s chair, its electronic structure provides a useful conceptual link (vide infra) to the shorter chain anions (n = 2–4). For the corresponding cis-trans isomer, which is isostructural with the closed shell $SSNSS^-$ anion [63,64], the energy gap is considerably less, both in the gas phase (26.1 kJ mol^{-1}) and in DMF (32.6 kJ mol^{-1}), but is still not a true minimum.

2.1.4. $S_6^{\bullet-}$

Here we have the unique advantage of experimental structural information on both the neutral molecule and its radical anion. The cyclic, chair-shaped structure of S_6, with D_{3d} symmetry and all neighboring bonds staggered, has been characterized crystallographically [65]; the observed S–S distance = 2.057(18) Å compares well with the value calculated here = 2.054 Å (Figure 3). In the corresponding radical anion $S_6^{\bullet-}$, identified in the crystal structure of the tetraphenylphosphonium salt $[Ph_4P][S_6]$, the cyclic chair shape is retained (Figure 3a), despite some disorder, but with two elongated S–S bonds = 2.634(4) Å [47]. In their report, however, the authors cautioned that the apparently high molecular symmetry (C_{2h}) observed for the anion might be dictated by the high lattice symmetry (space group $C2/c$), and provided BP86/TZ2P results indicating that a distorted chair structure (Figure 3b) with C_2 symmetry was actually more stable.

From a theoretical perspective, one-electron reduction of the high-symmetry geometry of neutral S_6 gives rise to an orbitally degenerate ground state for the resulting radical anion $S_6^{\bullet-}$. Thus, when using D_{3h} symmetry constraints as a starting point for a geometry optimization, the symmetric chair immediately breaks symmetry and undergoes a first-order Jahn–Teller distortion [61] to C_{2h} symmetry, affording two elongated S–S bonds, calculated here = 2.357 Å (Figure 3a), somewhat shorter than that observed experimentally. However, as observed earlier, while this centrosymmetric C_{2h} structure represents a stationary point it is not an energy minimum. Upon release of symmetry constraints, it undergoes a second-order distortion to the C_2 modification (Figure 3b), in which one of the two elongated S–S bonds in the C_{2h} geometry stretches further to 2.823 Å, a result in accord with the earlier DFT work [47]. By our calculations the energy difference between the C_{2h} and C_2 structures is large (22.5 kJ mol^{-1}), even in the gas phase, and increases to 27.5 kJ mol^{-1} with the inclusion of PCM (μ = 0 in the C_{2h} form).

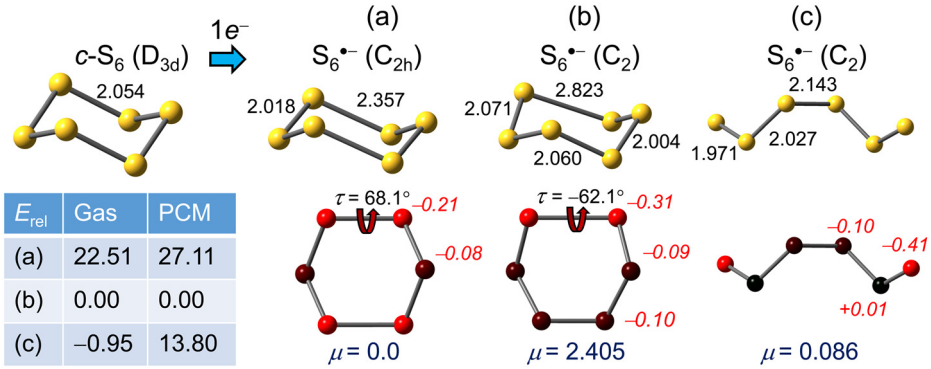

E_{rel}	Gas	PCM
(a)	22.51	27.11
(b)	0.00	0.00
(c)	−0.95	13.80

Figure 3. (U)PBE0/D3/def2-QZVP optimized geometries (distances in Å) for $S_6^{\bullet-}$, with Mulliken charges (in italics) and dipole moments (μ) in Debye. Relative gas phase and PCM (=DMF) corrected total energies E_{rel} are in kJ mol^{-1}.

In addition to the nominally closed-ring variants for $S_6^{\bullet-}$ several open chain options have been considered. Of these, we find the lowest energy C_2 structure (Figure 3c), which can be converted into the *quasi*-cyclic form by a ca. 180° rotation about the central S–S bond, constitutes a true minimum. Predictably, in the gas phase the total energies of the two rotamers are almost identical, but in accord with the low dipole moment of the open chain form the balance changes sharply in favor of the ring structure when the PCM is included.

2.1.5. $S_7^{\bullet-}$

Neutral S_7 possesses a chair-like structure with C_s symmetry [66,67], with the unique mirror-bisected bond lengthened to 2.18 Å (calculated here = 2.171 Å) by the effects of lone-pair repulsion occasioned by the eclipsed alignment of the neighboring bonds, as seen in *c*-S_5. In the structure of the global energetic minimum for $S_7^{\bullet-}$ the cyclic chair motif found in the neutral molecule is retained, but the already weakened mirror-bisected linkage is lengthened to 2.946 Å in the radical anion (Figure 4a), with the associated Mulliken charge densities heavily localized on the two sulfurs linked by the weakened bond.

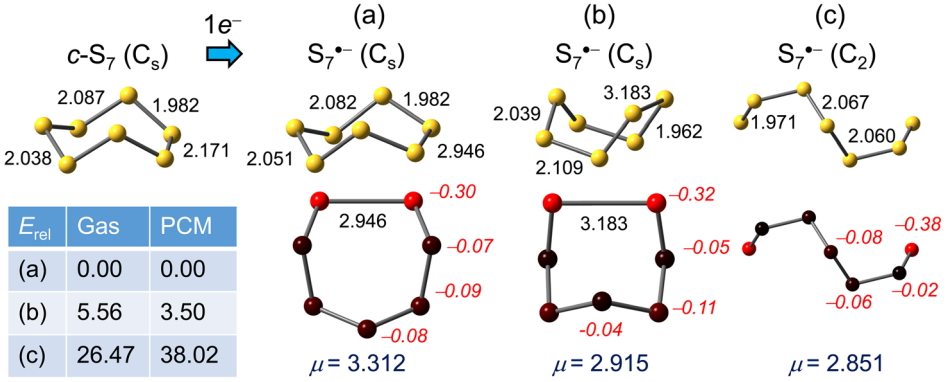

E_{rel}	Gas	PCM
(a)	0.00	0.00
(b)	5.56	3.50
(c)	26.47	38.02

Figure 4. (U)PBE0/D3/def2-QZVP optimized geometries (distances in Å) for $S_7^{\bullet-}$, with Mulliken charges (in italics) and dipole moments (μ) in Debye. Relative gas phase and PCM (=DMF) corrected total energies E_{rel} are in kJ mol^{-1}.

Not surprisingly, a boat-shaped conformation (Figure 4b), in which the unique S–S bond is a little longer (3.183 Å) than in the chair, is also possible. This feature may be of relevance to optical properties, as its relative energy lies only slightly above that of the chair in both the gas phase and solution, so that the two conformers may coexist in equilibrium in solution. Outside of this pair of *quasi*-cyclic structures there is an open chain variant with C_2 symmetry (Figure 4c). It represents a local energy minimum, but is significantly less stable than the chair/boat structures in the gas phase, the gap increasing when PCM is invoked.

2.1.6. $S_8^{\bullet-}$

The eight-membered ring found in orthorhombic α-sulfur displays a classic crown conformation with D_{4d} symmetry, with all neighboring bonds (measured at 2.055(2) Å, calculated here = 2.044 Å) mutually staggered [68]. The structural changes accompanying formation of $S_8^{\bullet-}$ follow a similar pattern to that seen for $S_6^{\bullet-}$. Addition of an electron to the cyclo-S_8 in D_{4d} symmetry affords a degenerate ground state for the resulting radical anion, thereby setting up a first order Jahn–Teller distortion [61], which in this case affords the "squeezed" C_{2v} crown geometry shown in Figure 5a.

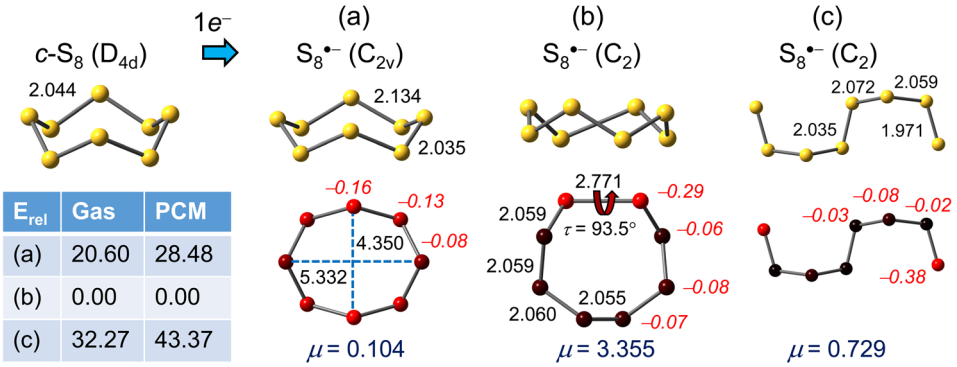

E_{rel}	Gas	PCM
(a)	20.60	28.48
(b)	0.00	0.00
(c)	32.27	43.37

Figure 5. (U)PBE0/D3/def2-QZVP optimized geometries (distances in Å) for $S_8^{\bullet-}$, with Mulliken charges (in italics) and dipole moments (μ) in Debye. Relative gas phase and PCM (=DMF) corrected total energies E_{rel} are in kJ mol^{-1}.

While this high-symmetry structure is not an energy minimum, the possibility of trapping it in a crystal lattice, as in the case of the C_{2h} form of $S_6^{\bullet-}$, is worthy of consideration. That being said, upon release of all symmetry constraints the C_{2v} structure evolves into a C_2 variant (Figure 5b) which, like the C_2 structure of $S_6^{\bullet-}$, displays one elongated S–S bond, calculated here = 2.771 Å. Outside of distorted crown geometries, there are few energetically viable alternatives. Of these, the open-chain C_2-symmetry motif (Figure 5c) represents the only true minimum, but its energy lies well above that of the C_2 crown. Given its relatively low polarity, inclusion of PCM further widens the energy gap.

In summary, the smaller members (n = 3, 4) of the polysulfide radical anion family adopt open chain structures, in part because they have no choice, as there is too much ring strain in the cyclic alternatives. That being said, when alternatives exist, as in the C_{2v} (cis) and C_{2h} (trans) options for $S_4^{\bullet-}$, solvent effects may well dictate the outcome, with the non-centric cis isomer being preferred in polar solvents and the centric trans isomer possibly being viable in non-polar solvents. For medium-sized rings, i.e., n = 5, 6, closed or broken-ring structures compete with open-chain variants, and again the choice may depend upon the polarity of the solvent employed, with polar environments or lattice constraints (for n = 6)) favoring the cyclic or *quasi*-cyclic modifications. In the following sections we focus on the structures most likely preferred in the latter environments. Finally, when n = 7 and 8, the stability of the cyclic structures clearly outranks the open-chain alternatives, regardless of solvent effects. Dynamic equilibria between cyclic and acyclic forms are unlikely, a conclusion which may have consequences for the mechanism of formation of S_8^{2-} [39].

2.2. Electronic Spectra

Using the polar-medium preferred geometries afforded by the unrestricted DFT calculations described above, single point TD-DFT calculations were performed on the radical anions $S_n^{\bullet-}$ (n = 2–8), to explore the number, nature and energies of the possible electronic excitations. A compilation of the relevant states, dominant orbital transitions, frequencies ν, wavelengths λ and oscillator strengths f is provided in Table 1.

Table 1. TD-DFT electronic excitations for $S_n^{\bullet-}$ (n = 2–8).

n in $S_n^{\bullet-}$	State	Excitation [a]	State	ν, eV	λ, nm	f
2 ($D_{\infty h}$)	$^2\Sigma_g$	$15\beta \rightarrow 17\beta$	$^2\Sigma_u$	3.177	390.3	0.0891
3 (C_{2v})	$^2B_1$	$24\beta \rightarrow 25\beta$	$^2B_2$	2.059	602.1	0.0920
4 (C_{2v})	$^2A_2$	$32\beta \rightarrow 33\beta$	$^2B_2$	1.242	998.3	0.0722
	$^2A_2$	$29\beta \rightarrow 33\beta$	$^2A_1$	3.533	351.0	0.0286
4 (C_{2h})	^2B_g	$32\beta \rightarrow 33\beta$	^2B_u	0.954	1299.5	0.0930
	^2B_g	$29\beta \rightarrow 33\beta$	^2A_g	3.578	346.6	0.0000 [b]
5 (C_{2v})	$^2B_1$	$40\beta \rightarrow 41\beta$	$^2B_2$	0.716	1732.3	0.0734
	$^2B_1$	$38\beta \rightarrow 41\beta$	$^2A_1$	2.583	479.9	0.0332
	$^2B_1$	$39\beta \rightarrow 42\beta$	$^2A_1$	3.519	352.4	0.1258
5 (C_s)	$^2A''$	$40\beta \rightarrow 41\beta$	$^2A''$	0.685	1809.6	0.0589
	$^2A''$	$38\beta \rightarrow 41\beta$	$^2A''$	1.940	638.2	0.0540
	$^2A''$	$37\beta \rightarrow 41\beta$	$^2A''$	2.653	467.4	0.0158
6 (C_{2h})	B_g	$49\alpha \rightarrow 50\alpha$	A_u	1.231	1007.3	0.0445
	B_g	$48\beta \rightarrow 49\beta$	B_g	1.978	627.5	0.0000 [b]
6 (C_2)	^2B	$48\beta \rightarrow 49\beta$	^2B	1.495	829.6	0.0611
	^2B	$46\beta \rightarrow 49\beta$	^2B	2.283	543.1	0.0308
7 (C_s chair)	$^2A''$	$56\beta \rightarrow 57\beta$	$^2A''$	1.749	708.7	0.1637
7 (C_s boat)	$^2A''$	$56\beta \rightarrow 57\beta$	$^2A''$	1.435	863.9	0.1729
8 (C_2 crown)	^2B	$64\beta \rightarrow 65\beta$	^2B	2.104	589.3	0.1551

[a] Dominant spin-orbital transitions from unrestricted TD-UωB97X-D/PCM/def2-QZVP calculations, with PCM = DMF. [b] Electric dipole forbidden.

As when dealing with geometrical trends, presentation and discussion of the results is developed according to the value of n, beginning with the three short-chain anions (n = 2–4), where the electronic excitations are all clearly $\pi \rightarrow \pi^*$. From there on (n = 5–8) the non-planar, distorted or broken-ring geometries militate against the use of conventional σ/π symmetry descriptors which usually aid with band assignments, but for n = 5 the calculated spectrum can still be rationalized by extension of the simple π-only model. Finally, the single elongated S–S linkages found in the *quasi*-cyclic structures (n = 6–8), which are broadly consistent with localized two-center three-electron (2c-3e) bonds, reminiscent of those found in transient organic disulfide radical anions $(RS\text{-}SR)^{\bullet-}$ [69,70], give rise to low energy excitations that are best described as $\sigma \rightarrow \sigma^*$ processes within the 2c-3e manifold.

2.2.1. $S_n^{\bullet-}$ (n = 2–4)

The origin of the electronic excitations in the short-chain radical anions $S_n^{\bullet-}$ (n = 2–4) can be readily understood with reference to the manifold of π-orbitals predicted by the classical Hückel molecular orbital (HMO) linear chain model [71,72], using linear arrays of overlapping sulfur 3*p*-orbitals as a basis set. For such systems the eigenvalues e_j are given by the analytical expression $e_j = \alpha + 2\beta \cos(j\pi/N + 1)$, where α and β are the respective Coulomb and resonance parameters, and N is the number of orbitals (atomic centers) in the chain. Schematic plots of the resulting π-energy levels and MOs are illustrated in Figure 6. Within this framework, a single $\pi \rightarrow \pi^*$ excitation ν_1 is expected for the diatomic anion $S_2^{\bullet-}$, with a slightly lower energy $n\pi \rightarrow \pi^*$ transition ν_1 anticipated for the triatomic chain $S_3^{\bullet-}$. Extrapolation to planar open chain $S_4^{\bullet-}$ systems suggests two excitations ν_1 and ν_2 are possible. Of these, ν_1 is predicted to occur at still lower energy, and its magnitude can be estimated by calibration against the known value of ν_1 for $S_3^{\bullet-}$ (λ_{max} = 615–620 nm in DMF or HMPA) [73]. Based on this simple model the first transition ν_1 in both isomers of $S_4^{\bullet-}$ is predicted to shift well beyond the visible region. For the cis (C_{2v}) isomer a second

excitation ν_2 is anticipated towards the UV region, while for the trans (C_{2h}) form ν_2 should not be observed at all, as it is symmetry-forbidden ($g \rightarrow g$).

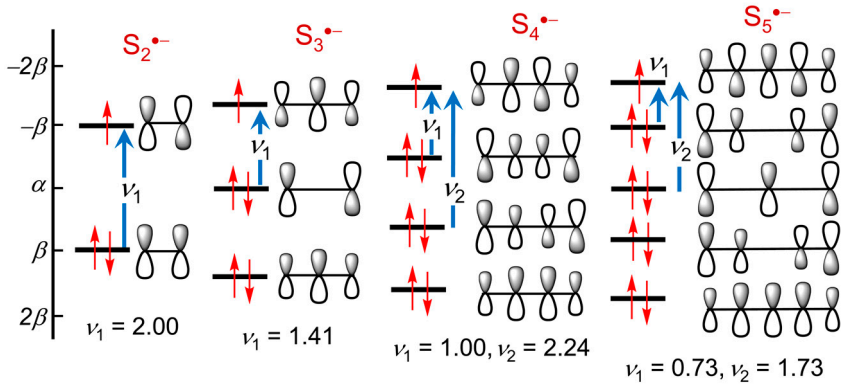

Figure 6. HMO energy levels for arrays of 3*p*-orbitals in model open chain $S_n^{\bullet-}$ (n = 2–5) radical anions; excitation energies ν_1, ν_2 are in units of β.

The TD-DFT calculations refine the qualitative predictions of the HMO model, confirming the nature of the expected transitions (Figure 7) and affording numerical estimates for the $\pi \rightarrow \pi^*$ excitation energies involved for both the cis (C_{2v}) and trans (C_{2h}) isomers. Calculated spectra for $S_n^{\bullet-}$ (n = 2–4) are shown in Figure 8.

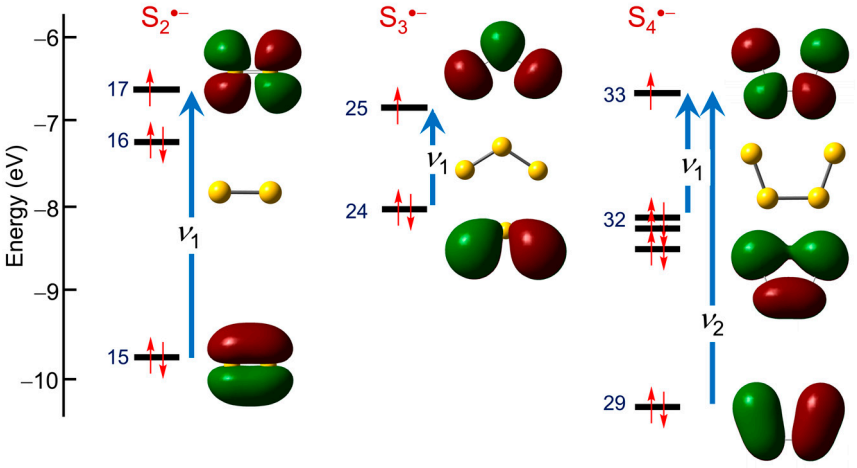

Figure 7. Spin-restricted TD-DFT frontier orbitals and excitations for $S_2^{\bullet-}$, $S_3^{\bullet-}$ and cis-$S_4^{\bullet-}$.

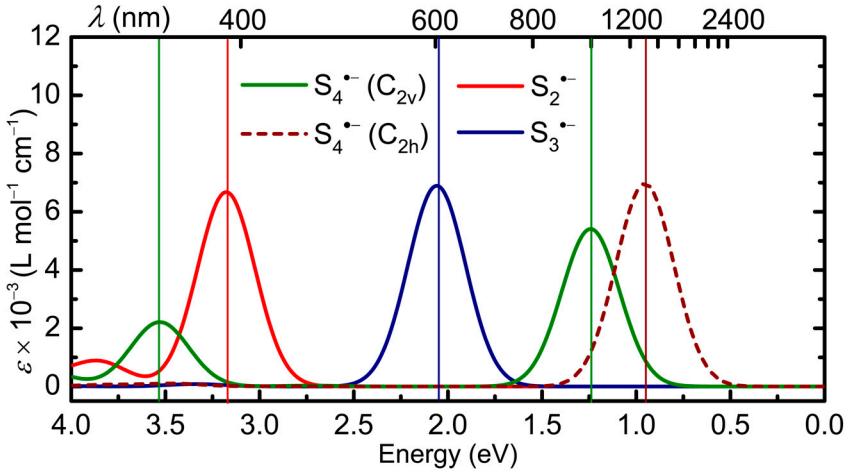

Figure 8. TD-DFT calculated electronic spectra in DMF of $S_n^{\bullet-}$ (n = 2, 3, 4), with HWHM = 0.18 eV; band assignments in Table 1.

The close correspondence between experimental λ_{max} values for n = 2 (~400 nm) [18] and n = 3 (615–620 nm in DMF or HMPA) [73] and those predicted by TD-DFT (Table 1) provide strong support for the choice of functional, and hence confidence in the calculated values for n = 4. The results for n = 4 are also in good qualitative agreement with those reported earlier [48,49], and thus help clarify some of the controversies surrounding the spectrophotometric identification of putative $S_4^{\bullet-}$ species. For both the cis and trans isomers, the first transition (ν_1, $32\beta \rightarrow 33\beta$) lies at or beyond the edge of the visible region (998 nm and 1300 nm, respectively), and for the cis isomer the second (ν_2, $29\beta \rightarrow 33\beta$) is predicted to have λ_{max} = 351 nm, placing it relatively close to $S_2^{\bullet-}$ and also many closed-shell dianionic species, e.g., S_3^{2-} [42], as well as other radical anions, e.g., $S_5^{\bullet-}$ (vide infra), from which it would be hard to distinguish. For the trans isomer, the second transition (ν_2, $29\beta \rightarrow 33\beta$) is symmetry-forbidden and has zero oscillator strength (f = 0). It will therefore display no signature at all in the visible region, regardless of its concentration in solution. In this light, assertions that $S_4^{\bullet-}$ has "never been observed" [39,43] by time-resolved spectroelectrochemistry perhaps deserve a second thought; absence of evidence is not evidence of absence.

2.2.2. $S_5^{\bullet-}$

TD-DFT analysis of the optical properties of $S_5^{\bullet-}$, using the coordinates of the chair-shaped C_s structure identified above as the most stable in polar media, affords an electronic spectrum (Figure 9) consisting of a series of bands spread across the entire visible and near-IR regions. However, in contrast to the three short-chain anions already discussed, the chair geometry of $S_5^{\bullet-}$ is not planar (although the molecule is bisected by a mirror plane), as a result of which rigorous characterization of individual orbitals and excitations between them according to their reflection symmetry in that plane, the classical σ/π classification, is no longer possible.

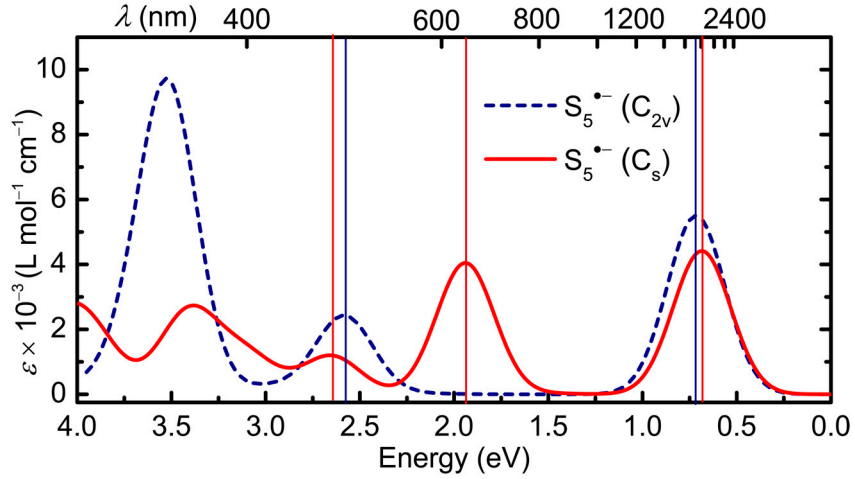

Figure 9. Calculated electronic spectrum of $S_5^{\bullet-}$ in DMF, in C_{2v} and C_s symmetry, with HWHM = 0.18 eV; band assignments in Table 1.

To resolve this difficulty, we examined the orbital make-up and electronic excitations found for the hypothetical planar variation with C_{2v} symmetry. While it is considerably less stable than the C_s form, by virtue of increased lone-pair repulsions, its higher symmetry allows for a clearer evaluation of its spectral signature, particularly in relation to the HMO open-chain model developed above. Indeed, it is immediately apparent by inspection of the frontier orbitals illustrated in Figure 10 that excitations $40\beta \rightarrow 41\beta$ and $38\beta \rightarrow 41\beta$ listed in Table 1 correspond to the two lowest energy $\pi \rightarrow \pi$ excitations ν_1 and ν_2 predicted by the HMO linear chain model with N = 5 (Figure 6). As expected, ν_1 lies deep into the near-IR (λ_{max} = 1732 nm), extending the shift to lower energy seen in cis and trans $S_4^{\bullet-}$ (λ_{max} = 998 and 1299 nm, respectively), with ν_2 likewise red-shifted to λ_{max} = 478 nm (from 351 nm in cis $S_4^{\bullet-}$). The third, very intense excitation, from $39\beta \rightarrow 42\beta$, with

λ_{max} = 352 nm, is not related to the chain model, nor even to a $\pi \rightarrow \pi$ transition, but is rather a lone-pair $\sigma \rightarrow \sigma$ process arising from the artificially enforced planarity of the structure.

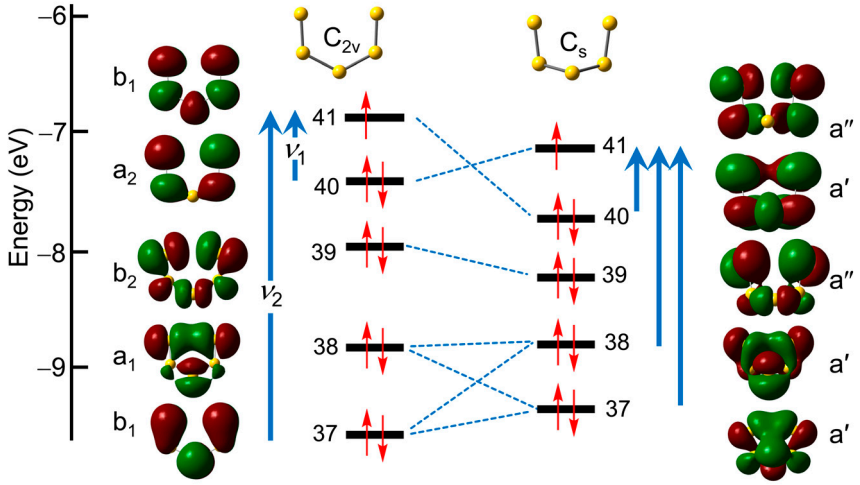

Figure 10. Correlation of spin-restricted TD-DFT frontier orbitals and electronic excitations for $S_5^{\bullet-}$ in C_{2v} and C_s symmetry.

With this information in hand, the origin of the optical signature of the C_s form emerges. The three lowest-lying states can each be described in terms a single dominant excitation from one of the doubly occupied molecular orbitals to the singly occupied molecular orbital (SOMO), that is, the lowest unoccupied molecular orbital (LUMO) for the unrestricted β-spins listed in Table 1. Moreover, correlation of the orbitals for the C_{2v} and C_s geometries confirms that the HMO chain model still applies, albeit more loosely because of the loss of planarity and consequent σ/π mixing. Thus, while the ordering of orbitals 40 and 41 is reversed, the first excitation, $40\beta \rightarrow 41\beta$ (λ_{max} = 1810 nm) can be considered a *quasi-* $\pi \rightarrow \pi$ transition related to ν_1 in the HMO model. The next two, $38\beta \rightarrow 41\beta$ (λ_{max} = 638 nm) and $37\beta \rightarrow 41\beta$ (λ_{max} = 467 nm), also involve heavily hybridized orbitals, but both are *quasi-* $\pi \rightarrow \pi$ processes that can be traced back to ν_2. The higher energy (>3 eV) absorptions comprise a series of less well-defined states arising from multiple excitations (see Table S2).

2.2.3. $S_6^{\bullet-}$

Addressing the optical properties of the $S_6^{\bullet-}$ anion presents a quandary. The crystallographic evidence indicates a symmetric chair structure with C_{2h} symmetry, while DFT optimizations point towards a distorted C_2 version. There are merits to both positions. In solution, and in the absence of environmental constraints, the lower-symmetry C_2 geometry is probably preferred, but the high space group symmetry of the $[Ph_4P][S_6]$ salt appears to hold the chair in the higher-symmetry C_{2h} form. In that light we have performed TD-DFT calculations on both options, using geometries taken from the respective structural optimizations.

As a first step, however, we focus on a qualitative model for describing the two elongated bonds in the symmetric structure. Building on the ideas developed earlier by Dehnicke and coworkers [47], Figure 11a illustrates the two strongly coupled σ and σ* orbitals arising from combinations of two S_3 fragments. A second-order Jahn–Teller distortion from C_{2h} to C_2 will give rise to mixing of the b_g SOMO and b_u LUMO, and a widening of the energy gap between them. Figure 11b refines this model, by showing the relevant spin-restricted Kohn–Sham orbitals and eigenvalues for the C_2 structure, that is, two heavily hybridized, but basically S–S σ-bonding, occupied orbitals (46 and 48), and a more localized σ*-orbital (49).

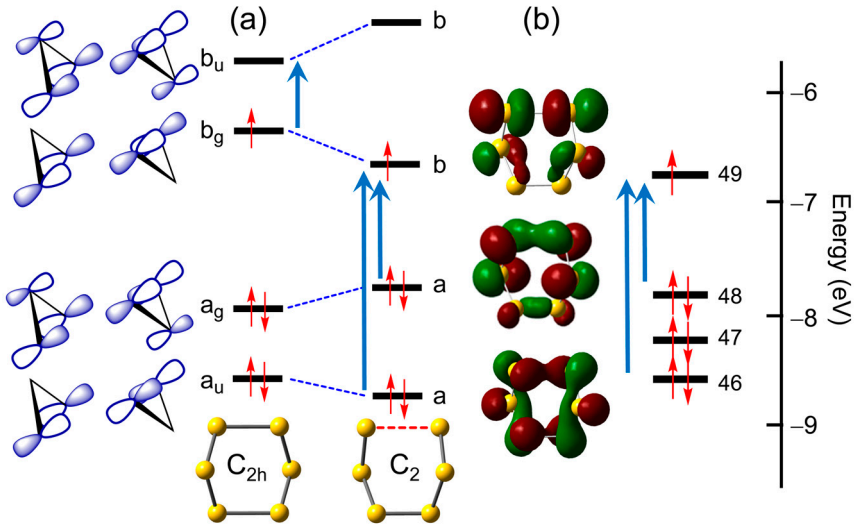

Figure 11. (**a**) Sketch of frontier orbital energies following distortion of $S_6^{\bullet-}$ from C_{2h} to C_2 symmetry. (**b**) Spin-restricted TD-DFT frontier orbitals and electronic excitations for $S_6^{\bullet-}$ in C_2 symmetry.

Given this conceptual framework, the optical signatures predicted for the two geometries are readily explained. As shown in Figure 12, the C_{2h} structure displays a single well-resolved band with λ_{max} = 1007 nm, which corresponds *not* to electron promotion from the HOMO to the SOMO, which is symmetry-forbidden ($g \rightarrow g$) in C_{2h}, but rather to the SOMO-to-LUMO excitation shown in Figure 11a ($49\alpha \rightarrow 50\alpha$, Table 1). In addition, there are a series of less well-defined states that give rise to a broad absorption that extends into the UV region.

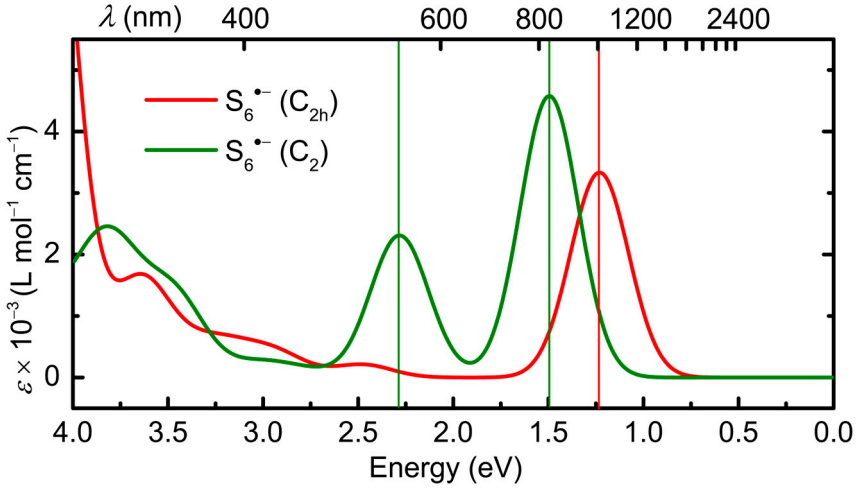

Figure 12. Calculated electronic spectrum of $S_6^{\bullet-}$ in DMF, in C_{2h} and C_2 symmetry, with HWHM = 0.18 eV; band assignments in Table 1.

For the distorted C_2 symmetry structure, the excited state manifold is quite different. Two bands are predicted in the visible and near-IR region (λ_{max} = 543 nm and 830), which arise primarily from the (now allowed) excitations, $46\beta \rightarrow 49\beta$ and $48\beta \rightarrow 49\beta$ (Table 1), from occupied orbitals to the SOMO, both of which are essentially $\sigma \rightarrow \sigma^*$ processes. As in the case of the C_{2h} geometry, there is a broad band extending into the UV region associated with a series of higher energy but less well-defined states.

In summary, the optical properties of both variations of the $S_6^{\bullet-}$ radical anion are associated with transitions associated with the lengthened S–S σ-bonds. In both its excited and ground states, the $S_6^{\bullet-}$ radical anion behaves like a cyclic molecule.

2.2.4. $S_7^{\bullet-}$ and $S_8^{\bullet-}$

The two largest radical anions (n = 7 and 8) are the easiest to analyze, as the structural perturbations occasioned by addition of an electron to the parent homocycles are small. Based on the structural parameters provided by the DFT optimizations of the chair and boat conformers of $S_7^{\bullet-}$, both of Cs symmetry, and of the C_2 distorted crown geometry of $S_8^{\bullet-}$, all three rings experience a lengthening of one of the S–S bonds, an effect which can best be described in terms of the formation of a largely localized 2c-3e σ-bond.

The TD-DFT calculations reinforce this picture, providing a description for the first excited state which involves promotion of an electron between the associated σ- and σ^*-orbitals of the 2c-3e manifold, that is, the β-spin HOMO and LUMO of the two conformers of $S_7^{\bullet-}$ ($56\beta \rightarrow 57\beta$) and those of $S_8^{\bullet-}$ ($64\beta \rightarrow 65\beta$) shown in Figure 13. These transitions give rise to single bands with large oscillator strength in the low-energy visible or near-IR region (Figure 14). As expected, there is a notable difference between the band maxima of the chair (λ_{max} = 709 nm) and boat (λ_{max} = 864 nm) conformations of $S_7^{\bullet-}$ which can be traced back to the longer S···S separation found in the latter (Figure 4).

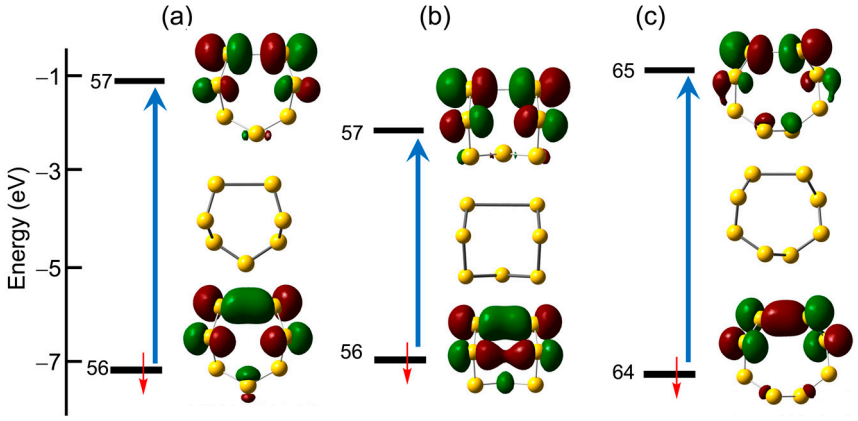

Figure 13. Unrestricted TD-DFT frontier orbitals and calculated $\sigma \rightarrow \sigma^*$ electronic excitations found for the (**a**) chair and (**b**) boat conformations of $S_7^{\bullet-}$ and (**c**) the C_2-distorted crown structure of $S_8^{\bullet-}$.

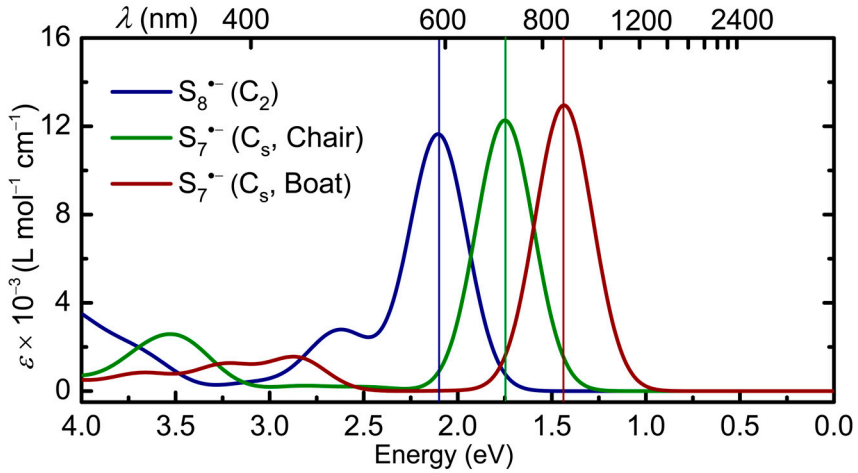

Figure 14. Calculated electronic spectra in DMF of $S_7^{\bullet-}$ (chair and boat conformations) and $S_8^{\bullet-}$, with HWHM = 0.18 eV; band assignments in Table 1 and Table S2.

The higher transition energy predicted for $S_8^{\bullet-}$ (λ_{max} = 589 nm) can be attributed to a similar effect, the shorter S···S separation stemming from the mutual staggering of the neighboring bonds and consequent relief from the effects of lone-pair repulsion. Secondary, less intense absorptions, with λ_{max} = 474 nm ($S_8^{\bullet-}$), 358 nm ($S_7^{\bullet-}$, chair) and 435 nm ($S_7^{\bullet-}$, boat), are also predicted. These are associated with poorly defined, higher-lying states (Table S2), but their presence may aid in identification. That being said, the strong low

energy $\sigma \rightarrow \sigma^*$ excitation, which dominates the spectrum of all three species, represents the most distinguishing optical feature.

3. Discussion

As indicated in the introduction, there are considerable differences of opinion as to when and where the radical anions $S_n^{\bullet -}$ (n = 4–8) might be found. While their participation in the multistep redox equilibria associated with the operation of sulfide/polysulfide photoconductor cells, alkali-metal/sulfur batteries, as well as in many biological and organic transformations, is frequently implied, their identification in these complex systems has, not surprisingly, proved elusive. Equally, extensive and detailed spectroscopic and spectroelectrochemical studies, utilizing a wide range of techniques (optical, IR, Raman, EPR spectra), have been unable to provide decisive answers.

The purpose of the present work has been two-fold. Firstly, the most stable structures of the putative radical anions $S_n^{\bullet -}$ (n = 4–8) in polar solvents have been identified using high-level DFT methods. Secondly, TD-DFT calculations, performed on the most stable structural candidates, have been used to map out the number, nature and energies of the photochemically accessible excited states for these species. Critical to the validity of this latter step was the ability to assess the numerical reliability of the methods used (choice of LC-functional for TD-DFT work) by comparison of the predicted excitation energies with experimental values for the well-known radical anions $S_2^{\bullet -}$ and $S_3^{\bullet -}$. Even so, we neither expect nor claim that the present TD-DFT calculated transition energies will provide a perfect match with experiment for the larger members of the series, especially for the low-energy (near-IR and beyond) excitations. Taken together, however, the results on the entire series of anions $S_n^{\bullet -}$ (n = 2–8) provide a frame of reference for distinguishing between different members of the family. Equally important, from an interpretational viewpoint, has been the use of the classical one-electron HMO chain model [74,75] to anticipate both the number and *approximate* energies of $\pi \rightarrow \pi$ transitions, again using $S_2^{\bullet -}$ and $S_3^{\bullet -}$ as reference points. The TD-DFT results suggest that the calculated spectra for $S_4^{\bullet -}$, and even $S_5^{\bullet -}$, can be effectively rationalized by this approach. By contrast, the low energy excitations predicted for the essentially cyclic structures of $S_n^{\bullet -}$ (n = 6–8) are best described in terms of $\sigma \rightarrow \sigma^*$ processes within a relatively localized 2c-3e manifold.

The availability of this information opens the door to the design of experimental strategies for the generation, observation and perhaps even isolation of the radical anions $S_n^{\bullet -}$ (n = 4–8). We begin by considering the seminal 1991 report by Rauchfuss and coworkers on the structure and spectroscopic properties of the open-chain octasulfide dianion S_8^{2-} in the absence of counterion pairing effects [48]. As noted earlier, these authors attributed the strong band with λ_{max} = 618 nm that emerged upon dilution of a solution of [Mn(*N*-MeIm)$_6$][S_8] (*N*-MeIm = *N*-methylimidazole) in *N*-MeIm to the presence of the radical anion $S_3^{\bullet -}$. At the time they rationalized the generation of $S_3^{\bullet -}$ in terms of a disproportionation of S_8^{2-} to $\frac{1}{4}S_8$ and S_6^{2-}, and subsequent dissociation of the latter, following the conventional interpretation of the electrochemistry community [35,49]. Other radical anions, notably $S_n^{\bullet -}$ (n = 4, 5), were not included in the analysis, in part because their optical signatures were unknown. Given the present TD-DFT results, however, the potential involvement of these seemingly missing radical anions can be examined. In particular, we consider the possibility that both might be formed, along with $S_3^{\bullet -}$, by either symmetric or asymmetric dissociation of the S_8^{2-} dianion, as indicated in Scheme 1. In addition to the overall thermodynamics of such processes [43], mechanistic considerations may also be important—how easy is it to rupture the distinct S–S bonds along the chain? In response to this question, we suggest that dissociation may proceed via four-center intermediates, as illustrated in Scheme 2. Indeed, in the case of symmetric dissociation, an example of a four-center π-dimer has been characterized crystallographically [21].

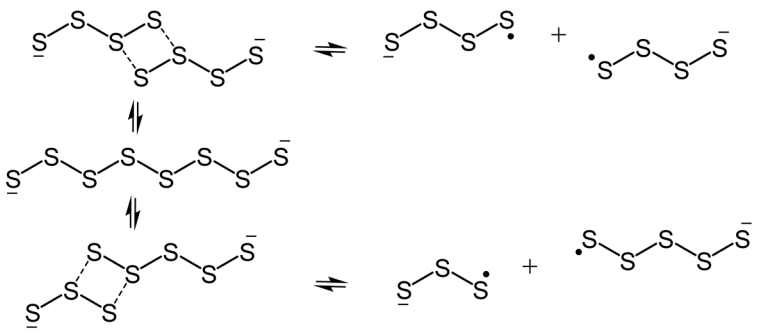

Scheme 2. Symmetric and asymmetric dissociation of S_8^{2-} to the radical anions $S_n^{\bullet-}$ (n = 3, 4, 5).

As an example of the spectroscopic ramifications of this interpretation, we compare in Figure 15 the experimental spectrum for the highly diluted solution of S_8^{2-}, as reported by Rauchfuss, with an equally weighted composite of the TD-DFT calculated spectra for $S_3^{\bullet-}$ and $S_5^{\bullet-}$, the two products of an *asymmetric* dissociation. In the mid-range visible region, the correspondence is remarkable, not only in terms of the overlap and coalescence of the two bands calculated for n = 3, 5, but also the presence of the weaker band near 480 nm which, on the present basis, may be assigned to n = 5 (calculated λ_{max} = 467 nm). Below 400 nm the match is less than ideal, but could be improved by inclusion into the composite of cis $S_4^{\bullet-}$ (calculated λ_{max} = 351 nm), the unique *symmetric* dissociation product. Alternatively, these higher energy absorptions may arise from *un*dissociated S_6^{2-}. That being said, the absence of bands attributable to $S_2^{\bullet-}$ or $S_6^{\bullet-}$ suggests dissociation of S_8^{2-} into these species does not occur to any great extent.

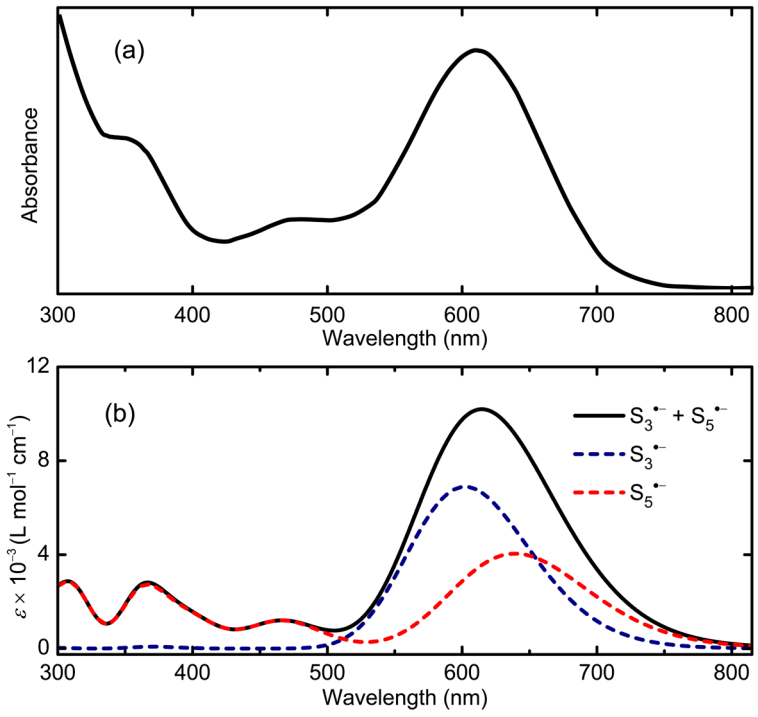

Figure 15. (**a**) Optical spectrum of 0.001 M solution of [Mn(*N*-MeIm)$_6$][S_8] in *N*-MeIm, reproduced from [48]; copyright American Chemical Society. (**b**) Calculated composite spectrum, with HWHM = 0.18 eV, for equally weighted mixture of $S_3^{\bullet-}$ and $S_5^{\bullet-}$ in DMF.

By itself, this single spectral deconvolution exercise does not constitute proof for multiple dissociation pathways, but critical support for the concept could be readily achieved by inspection of the near-IR region of dilute solutions of S_8^{2-}, where one or both of the low-energy (ν_1) bands of $S_4^{\bullet-}$ and $S_5^{\bullet-}$ should be present. Moreover, similar spectroscopic analysis at high dilution of solutions of salts of the known hepta- and hexasulfide dianions

S_7^{2-} and S_6^{2-} should reveal predicable patterns of radical anions, the former affording $S_3^{\bullet-}$ and $S_4^{\bullet-}$ (but possibly not $S_5^{\bullet-}$) and the latter specifically $S_3^{\bullet-}$; indeed, for S_6^{2-} this result has already been confirmed [48]. In the same way, observation of the cyclic radical anions $S_n^{\bullet-}$ (n = 6–8) may be possible, by examination of highly diluted solutions of long chain dianions such S_{10}^{2-} [49] and S_{12}^{2-} [50].

In addition to routes to the radical anions which rely solely on dissociative equilibria between radical anions and closed-shell dianions, direct chemical synthesis may be possible, as in the case of the radical anion salt $[Ph_4P][S_6]$, which was prepared by the rather unusual reaction of H_2S and Me_3SiN_3 in the presence of $[Ph_4P][N_3]$ [52]. If this procedure could be adapted to incorporate the use of other bulky cations, e.g., PPN^+, different crystal morphologies might be generated. That being the case, would the structure of the resulting anion be constrained to C_{2h} symmetry, as in $[Ph_4P][S_6]$, or display the more stable distorted C_2 shape? Even in the solid state, the expected optical signatures (Figure 12) are predicted to be quite different. Alternatively, not only $S_6^{\bullet-}$ but also $S_7^{\bullet-}$ and $S_8^{\bullet-}$ could be accessible by electrochemical reduction of the appropriate neutral allotrope [76–78]. The latter two anions have very distinct optical profiles, although we add the caveat that the footprint of $S_8^{\bullet-}$ may easily be confused with that of $S_3^{\bullet-}$.

Chemical reduction methods, for example using organometallic reducing agents such as cobaltocene, which is known to afford salts of closed [79] and open shell anions [80] with sulfur-based electron acceptors, may also provide access to salts of $S_8^{\bullet-}$. In this connection Woollins et al. obtained the salt $[Cp_2Co][S_3N_3]$ from the reaction of S_4N_4 with cobaltocene in THF [81]. This transformation probably involves the initial generation of the radical anion $S_4N_4^{\bullet-}$, known from electrochemical studies to be formed by one-electron reduction of S_4N_4, which then undergoes ring contraction to produce $S_3N_3^-$ [77].

Just as chemical oxidation of cyclo-S_8 has afforded the radical cation $S_8^{\bullet+}$ [78], treatment of salts of the dianions S_7^{2-} [82] and S_8^{2-} [47,48] with mild oxidants, e.g., iodine or *N*-bromosuccinimide, might well yield the corresponding radical anions $S_7^{\bullet-}$ and $S_8^{\bullet-}$. An alternative to chemical oxidation is the use of photolysis to generate polysulfide radical anions from the corresponding dianions. This approach is based on the recent work of Chiba and co-workers on the production of polysulfide radical anions $S_n^{\bullet-}$ (n = 3, 4) [25–27] via photolysis of the polysulfide dianion S_4^{2-}, as well as on insights provided by investigations into the photoelectrochemical oxidation of S^{2-} by metal-sulfide quantum dots [14,15].

Last, but not least, we acknowledge the role that serendipity has played in the advancement of the chemistry of polysulfide radical anions. For example, the procedures used to achieve the isolation and characterization of $S_6^{\bullet-}$ [52] and of the π-dimer of $S_4^{\bullet-}$ [21] would have been difficult to predict a priori, but their somewhat fortuitous discovery strengthens the conviction that continued exploration will yield new insights. Towards that end the present results may prove useful.

4. Computational Methods

Unrestricted density functional theory (DFT) calculations were performed with the Gaussian 16 suite of programs [74], using the default ultrafine integration grids. Geometry optimizations employed the hybrid-adapted Perdew–Burke–Ernzerhof functional (PBE0) [75,83] and Ahlrichs' quadruple-ξ valence def2-QZVP basis set [84], without additional diffuse functions [85] but with Grimme's empirical correction (D3) [81,86] included to account for possible dispersion effects [87]. For most anions several geometries, both cyclic and acyclic, were considered, and wherever a stationary point was located a full vibrational analysis was performed to determine whether or not it corresponded to a true energy minimum. Preferred geometries were further optimized with the inclusion of the polarized continuum model (PCM) [88] to account for the effects of solvation, dimethylformamide (DMF) being set as a representative polar solvent. Listings of total energies, vibrational frequencies and cartesian coordinates, with and without PCM, are provided in the SI.

The optical properties of the polysulfide radical anions were explored using single point unrestricted time-dependent (TD) DFT calculations, with the same def2-QZVP basis

set and PCM included. The use of several long range corrected (LC) functionals, which are known to provide reasonable estimates of low energy (charge transfer, Rydberg-like) excitations in molecular species [89,90], including radicals [91] and sulfur-containing radical anions [92], was explored. The best results, reported here, employed the empirical dispersion-corrected density functional ωB97XD [93], which is well recognized for its overall performance [94]. All tabulated excitation energies refer to spin-unrestricted calculations, but for ease of visualization some of the orbital energy diagrams are based on spin-restricted wavefunctions. All spectral plots, prepared using Gaussview 6 [95], employed Gaussian band shapes with the half-width at half maximum (HWHM) value set at 0.18 eV. The associated extinction coefficients were derived using routines available within Gaussview. Kohn–Sham wavefunctions were also plotted using Gaussview.

5. Conclusions

The DFT and TD-DFT calculations reported here represent the first comprehensive attempt both to predict and to rationalize the optical properties of the entire family of polysulfide radical anions $S_n^{\bullet-}$ (n = 2–8). Our results confirm earlier predictions [52,53] that the first $\pi \rightarrow \pi$ transition for both the cis (C_{2v}) and slightly less stable trans (C_{2h}) isomers of $S_4^{\bullet-}$ should occur in the near-IR region. However, a second $\pi \rightarrow \pi$ transition at around 350 nm is expected for the cis isomer of $S_4^{\bullet-}$. Based on Seel's early results [19,20], a band near 490 nm has often been attributed to this species, but these conclusions are questionable [3]. At least in dilute solution this band may originate from $S_5^{\bullet-}$, the most stable form of which possesses an acyclic structure with C_s symmetry, and is predicted to display three optical absorption bands, two in the visible and one in the near-IR region.

The $S_6^{\bullet-}$ radical anion is an interesting and unique example of a polysulfide radical anion that has been structurally characterized in the solid state. In the ion-separated salt $[Ph_4P][S_6]$ the anion displays a cyclic structure (C_{2h} symmetry) with two long S–S bonds [51], while DFT geometry optimization points to a distorted cyclic structure (C_2 symmetry) with one long S–S bond as a more stable arrangement. The predicted electronic spectra for these two forms are very different, with λ_{max} = 1007 nm vs. 830 and 543 nm, respectively.

To date the heptasulfide radical anion $S_7^{\bullet-}$ has received scant attention, but the present DFT results point to a cyclic structure with two energetically similar conformers, chair and boat (Cs symmetry), both displaying one long S−S bond best described in terms of a localized 2c-3e σ-interaction. Electronic excitation within this manifold gives rise to a strong visible/near-IR absorption with calculated values of λ_{max} = 709 nm and 864 nm for chair and boat, respectively. The octasulfide radical anion $S_8^{\bullet-}$, which carries particular significance as the initial product of the electrochemical reduction of cyclo-S_8 [3], is also predicted to possess a distorted cyclic structure (C_2 symmetry) exhibiting, like $S_7^{\bullet-}$, a single elongated 2c-3e S−S bond. The associated $\sigma \rightarrow \sigma^*$ excitation generates a strong visible absorption band with a calculated λ_{max} = 589 nm.

Supplementary Materials: The following supporting information (21 pages total) can be downloaded at: https://www.mdpi.com/article/10.3390/molecules28155654/s1, Figure S1: Optimized geometrical parameters; Table S1: Total electronic energies; Table S2: Excitation energies, oscillator strengths and orbital contributions; Tables S3–S11: Gaussian archive entries; Tables S12–S17: Frequency calculations.

Author Contributions: The two authors contributed equally to this work. All authors have read and agreed to the published version of the manuscript.

Funding: Financial support from NSERC (Canada).

Data Availability Statement: Details of the computational data are in the Supplementary Materials.

Conflicts of Interest: The authors declare no conflict of interest.

References

1. Chivers, T. Ubiquitous trisulphur radical ion $S_3^{\bullet-}$. *Nature* **1974**, *252*, 32–33. [CrossRef]
2. Steudel, R. Inorganic polysulfides S_n^{2-} and radical anions $S_n^{\bullet-}$. In *Elemental Sulfur and Sulfur-Rich compounds II. Topics in Current Chemistry*; Steudel, R., Ed.; Springer: Berlin/Heidelberg, Germany, 2003; Volume 231, pp. 127–152.
3. Steudel, R.; Chivers, T. The role of polysulfide dianions and radical anions in the chemical, physical and biological sciences, including sulfur-based batteries. *Chem. Soc. Rev.* **2019**, *48*, 3279–3319. [CrossRef] [PubMed]
4. Laitinen, R.S.; Oilunkaniemi, R.; Chivers, T.; McGeachie, L.; Kelly, P.F.; King, R.S.P. Polychalcogen molecules, ligands, and ions Part 2: Catenated acyclic molecules, ions, and p-block element derivatives. In *Reference Module in Chemistry, Molecular Sciences and Chemical Engineering*; Elsevier: Amsterdam, The Netherlands, 2023; pp. 970–1020.
5. Zheng, D.; Wang, G.; Liu, D.; Si, J.; Ding, T.; Qu, D.; Yang, X.; Qu, D. The progress of Li−S batteries—Understanding of the sulfur redox mechanism: Dissolved polysulfide ions in the electrolytes. *Adv. Mater. Technol.* **2018**, *3*, 1700233. [CrossRef]
6. Zhao, E.; Nie, K.; Yu, X.; Hu, Y.-S.; Wang, F.; Xiao, J.; Li, H.; Huang, X. Advanced characterization techniques in promoting mechanism understanding for lithium-sulfur batteries. *Adv. Func. Mater.* **2018**, *28*, 1707543. [CrossRef]
7. Zhang, G.; Zhang, Z.-W.; Peng, H.-J.; Huang, J.-Q.; Zhang, Q. A toolbox for lithium-sulfur research: Methods and protocols. *Small Methods* **2017**, *1*, 1700134. [CrossRef]
8. Song, P.; Rao, W.; Chivers, T.; Wang, S.-Y. Applications of trisulfide radical anion $S_3^{\bullet-}$ in organic chemistry. *Org. Chem. Front.* **2023**, *10*, 3378–3401. [CrossRef]
9. Bogdándi, V.; Ida, T.; Sutton, T.R.; Bianco, C.; Ditrói, T.; Koster, G.; Henthorn, H.A.; Minnion, M.; Toscano, J.P.; van der Vliet, A.; et al. Speciation of reactive sulfur species and their reactions with alkylating agents: Do we have any clue about what is present in the cell? *Br. J. Pharmacol.* **2019**, *176*, 646–670. [CrossRef] [PubMed]
10. Cortese-Krott, M.M.; Kuhnle, G.G.C.; Dyson, A.; Fernandez, B.O.; Grman, M.; DuMond, J.F.; Barrow, M.P.; McLeod, G.; Nakagawa, H.; Ondrias, K.; et al. Key bioactive reaction products of the NO/H_2S interaction are S/N hybrid species, polysulfides, and nitroxyl. *Proc. Natl. Acad. Sci. USA* **2015**, *112*, E4651–E4660. [CrossRef] [PubMed]
11. Pokrovski, G.S.; Dubrovinsky, L.S. The $S_3^{\bullet-}$ ion is stable in geological fluids at elevated temperatures and pressures. *Science* **2011**, *331*, 1052–1054. [CrossRef] [PubMed]
12. Pokrovski, G.S.; Kokh, M.A.; Guillaume, D.; Borisova, A.Y.; Gisquet, P.; Hazemann, J.-L.; Lahera, E.; Del Net, W.; Proux, O.; Testemale, D.; et al. Sulfur radical species form gold deposits on earth. *Proc. Nat. Acad. Sci. USA* **2015**, *112*, 13484–13489. [CrossRef]
13. Pokrovski, G.S.; Kokh, M.A.; Desmaele, E.; Laskar, C.; Bazarkina, E.F.; Borisova, A.Y.; Testemale, D.; Hazemann, J.-L.; Vuilleumier, R.; Ferlat, G.; et al. The trisulfur radical ion $S_3^{\bullet-}$ controls platinum transport by hydrothermal fluids. *Proc. Nat. Acad. Sci. USA* **2021**, *118*, e2109768118. [CrossRef] [PubMed]
14. Li, X.; McNaughter, P.D.; O'Brien, P.; Minamimoto, H.; Murakoshi, K. Photoelectrochemical formation of polysulfide at PbS QD-sensitized plasmonic electrodes. *J. Phys. Chem. Lett.* **2019**, *10*, 5357–5363. [CrossRef] [PubMed]
15. Chakrapani, V.; Baker, D.; Kamat, P.V. Understanding the role of the sulfide redox couple (S^{2-}/S_n^{2-}) in quantum dot-sensitized solar cells. *J. Am. Chem. Soc.* **2011**, *133*, 9607–9615. [CrossRef]
16. Reinen, D.; Lindner, G.-G. The nature of the chalcogen colour centres in ultramarine type solids. *Chem. Soc. Rev.* **1999**, *28*, 75–84. [CrossRef]
17. Chukanov, N.V.; Sapozhnikov, A.N.; Shendrik, R.Y.; Vigasina, M.F.; Steudel, R. Spectroscopic and crystal-chemical features of sodalite-group minerals from gem lazurite deposits. *Minerals* **2020**, *10*, 1042. [CrossRef]
18. Chivers, T.; Elder, P.J.W. Ubiquitous trisulfur radical anion: Fundamentals and applications in materials science, electrochemistry, analytical chemistry, and geochemistry. *Chem. Soc. Rev.* **2013**, *42*, 5996–6005. [CrossRef]
19. Seel, F. Polysulfide radical anions. *Angew. Chem. Int. Ed.* **1973**, *12*, 420–421. [CrossRef]
20. Seel, F.; Guttler, H.-J.; Simon, G.; Wieckowski, A. Colored sulfur species. *Pure Appl. Chem.* **1977**, *49*, 45–54. [CrossRef]
21. Schwamm, R.J.; Lein, M.; Coles, M.P.; Fitchett, C.M. Bismuth (III) complex of the $S_4^{\bullet-}$ radical anion: Dimer formation via pancake bonds. *J. Am. Chem. Soc.* **2017**, *139*, 16490–16493. [CrossRef] [PubMed]
22. Clark, R.J.H.; Dines, T.J.; Kurmoo, M. The nature of the sulfur chromophore in ultramarine blue, green, violent, and pink and of the selenium chromophore in ultramarine selenium. Characterization of radical anions by electronic and resonance Raman spectroscopy and the determination of their excited-state geometries. *Inorg. Chem.* **1983**, *22*, 2766–2772.
23. Rauh, R.D.; Shuker, F.S.; Marston, J.M.; Brummer, S.B. Formation of lithium polysulfides in aprotic media. *J. Inorg. Nucl. Chem.* **1977**, *39*, 1761–1766. [CrossRef]
24. Li, H.; Tang, X.; Pang, J.H.; Wu, X.; Yeow, E.K.L.; Wu, J.; Chiba, S. Polysulfide anions as visible light photoredox catalysts for aryl cross-couplings. *J. Am. Chem. Soc.* **2021**, *143*, 481–487. [CrossRef] [PubMed]
25. Li, H.; Liu, Y.; Chiba, S. Leveraging of sulfur anions in photoinduced molecular transformations. *JACS Au* **2021**, *1*, 2121–2129. [CrossRef] [PubMed]
26. Li, H.; Liu, Y.; Chiba, S. Anti-Markovnikov hydroarylation of alkenes via polysulfide anion photocatalysis. *Chem. Commun* **2021**, *57*, 6264–6267. [CrossRef] [PubMed]
27. Li, H.; Chiba, S. Synthesis of α-tertiary amines by polysulfide anions photocatalysis via single-electron transfer and hydrogen atom transfer in relays. *Chem. Catal.* **2022**, *2*, 1128–1142. [CrossRef]

28. Hagen, M.; Schiffels, P.; Hammer, M.; Dörfler, S.; Tübke, J.; Hoffmann, M.; Althues, H.; Kaskel, S. In-situ Raman investigation of polysulfide formation in Li-S cells. *J. Electrochem. Soc.* **2013**, *160*, A1205–A1215. [CrossRef]
29. Clark, R.J.H.; Cobbold, D.G. Characterization of sulfur radical anions in solutions of alkali polysulfides in DMF and HMPA and in the solid state in ultramarine blue, green, and red. *Inorg. Chem.* **1978**, *17*, 3169–3174. [CrossRef]
30. Wu, H.-L.; Huff, L.A.; Gewirth, A.A. In-situ Raman spectroscopy of sulfur speciation in Li-S batteries. *Appl. Mater. Interfaces* **2015**, *7*, 1709–1719. [CrossRef]
31. Levillain, E.; Leghié, P.; Gobeltz, N.; Lelieur, J.-P. Identification of the $S_4^{\bullet -}$ radical anion in solution. *New J. Chem.* **1997**, *21*, 335–341.
32. Wujcik, K.H.; Wang, D.R.; Raghunathan, A.; Drake, M.; Pascal, T.A.; Prendergast, D.; Balsara, N.P. Lithium polysulfide radical anions in ether-based solvents. *J. Phys. Chem. C* **2016**, *120*, 18403–18410, and references cited therein. [CrossRef]
33. Chukanov, N.V.; Shendrik, R.Y.; Vigasina, M.F.; Pekov, I.V.; Sapozhnikov, A.N.; Shcherbakov, V.D.; Varlamov, D.A. Crystal chemistry, isomorphism, and thermal conversions of extra-framework components in sodalite-group minerals. *Minerals* **2022**, *12*, 887. [CrossRef]
34. Merritt, M.V.; Sawyer, D.T. Electrochemical reduction of elemental sulfur in aprotic solvents. Formation of a stable $S_8^{\bullet -}$ species. *Inorg. Chem.* **1970**, *9*, 211–215. [CrossRef]
35. Martin, R.P.; Doub, W.H.; Roberts, J.L.; Sawyer, D.T. Further studies of the electrochemical reduction of sulfur in aprotic solvents. *Inorg. Chem.* **1973**, *12*, 1921–1924. [CrossRef]
36. Bonnaterre, R.; Cauquis, G. Spectrophotometric study of the electrochemical reduction of sulphur in organic media. *J. Chem. Soc. Chem. Commun.* **1972**, 293–294. [CrossRef]
37. Manan, N.S.A.; Aldous, L.; Alias, Y.; Murray, P.; Yellowlees, L.J.; Lagunas, M.C.; Hardacre, C. Electrochemistry of sulfur and polysulfides in ionic liquids. *J. Phys. Chem. B* **2011**, *115*, 13873–13879. [CrossRef]
38. Jung, Y.; Kim, S.; Kim, B.S.; Han, D.H.; Park, S.M.; Kwak, J. Effect of organic solvents and electrode materials on electrochemical reduction of sulfur. *J. Electrochem. Soc.* **2008**, *3*, 566–577. [CrossRef]
39. Gaillard, F.; Levillain, E.; Lelieur, J.-P. Polysulfides in DMF: Only the radical anions $S_3^{\bullet -}$ and $S_4^{\bullet -}$ are reducible. *J. Electroanal. Chem.* **1997**, *432*, 129–138. [CrossRef]
40. Evans, A.; Montenegro, M.I.; Pletcher, D. The mechanism for the cathodic reduction of sulphur in DMF: Low temperature voltammetry. *Electrochem. Commun.* **2001**, *3*, 514–518. [CrossRef]
41. Levillain, E.; Gaillard, F.; Leghié, P.; Demortier, A.; Lelieur, J.-P. On the understanding of the reduction of sulfur (S_8) in dimethylformamide (DMF). *J. Electroanal. Chem.* **1997**, *420*, 167–177. [CrossRef]
42. Leghié, P.; Lelieur, J.-P.; Levillain, E. Final comment on Reply to "Comments on the mechanism of the electrochemical reduction of sulphur in DMF". *Electrochem. Commun.* **2002**, *4*, 406–411. [CrossRef]
43. Steudel, R.; Steudel, Y. Polysulfide chemistry in sodium-sulfur batteries and related systems: A computational study by G3X(MP2) and PCM calculations. *Chem. Eur. J.* **2013**, *19*, 3162–3176. [CrossRef] [PubMed]
44. Kim, B.-S.; Park, S.-M. In situ spectroelectrochemical studies on the reduction of sulfur in dimethyl sulfoxide solutions. *J. Electrochem. Soc.* **1993**, *140*, 115–122. [CrossRef]
45. Han, D.-H.; Kim, B.-S.; Choi, S.-J.; Jung, Y.; Kwak, J.; Park, S.-M. Time-resolved in situ spectroelectrochemical study on reduction of sulfur in DMF. *J. Electrochem. Soc.* **2004**, *151*, E283–E290. [CrossRef]
46. Cuisinier, M.; Hart, C.; Balusubramanian, M.; Garsuch, A.; Nazar, L.F. Radical or not radical: Revisiting lithium-sulfur electrochemistry in non-aqueous solvents. *Adv. Energy Mater.* **2015**, *5*, 1401801. [CrossRef]
47. Schliephke, A.; Falius, H.; Buchkremer-Hermanns, H.; Bottcher, P. Preparation and crystal structure of the bis(triethylammonium) octasulfide, $[HN(C_2H_5)_3]_2S_8$. *Z. Naturforsch.* **1988**, *43b*, 21–24.
48. Dev, S.; Ramli, E.; Rauchfuss, T.B.; Wilson, S.R. Synthesis and structure of $[M(N\text{-methylimidazole})_6]S_8$ (M = Mn, Fe, Ni, Mg). Polysulfide salts prepared by the reaction of N-methylimidazole + metal powder + sulfur. *Inorg. Chem.* **1991**, *30*, 2514–2519. [CrossRef]
49. Fujinaga, T.; Kuwamoto, T.; Okazaki, S.; Hojo, M. Electrochemical Reduction of Elemental Sulfur in Acetonitrile. *Bull. Chem. Soc. Jpn.* **1980**, *53*, 2851–2855. [CrossRef]
50. Mondal, M.K.; Zhang, L.; Feng, Z.; Tang, S.; Feng, R.; Zhao, Y.; Tan, G.; Ruan, H.; Wang, X. Tricoordinate pnictogen-centered radical anions: Isolation, characterization, and reactivity. *Angew. Chem. Int. Ed.* **2019**, *58*, 15829–15833. [CrossRef]
51. Liebing, P.; Kühling, M.; Swanson, C.; Feneberg, M.; Hilfert, L.; Goldhahn, R.; Chivers, T.; Edelmann, F.T. Catenated and spirocyclic polychalcogenides from potassium carbonate and elemental chalcogens. *Chem. Commun.* **2019**, *55*, 14965–14967. [CrossRef] [PubMed]
52. Neumüller, B.; Schmock, F.; Kirmse, R.; Voigt, A.; Diefenbach, A.; Bickelhaupt, F.M.; Dehnicke, K. $(Ph_4P)S_6$—A compound containing the cyclic radical anion $S_6^{\bullet -}$. *Angew. Chem. Int. Ed.* **2002**, *39*, 4580–4582. [CrossRef]
53. Fabian, J.; Komiha, N.; Linguerri, R.; Rosmus, P. The absorption wavelengths of sulfur chromophores of ultramarines calculated by TD-DFT. *J. Mol. Struct. THEOCHEM* **2006**, *801*, 63. [CrossRef]
54. Rejmak, P. Computational refinement of the puzzling red tetrasulfur chromophore in ultramarine pigments. *PhysChemChemPhys* **2020**, *22*, 22684–22698. [CrossRef]
55. Hunsicker, S.; Jones, R.O.; Ganteför, G. Rings and chains in sulfur cluster anions S^- to S_9^-: Theory (simulated annealing) and experiment (photoelectron detachment). *J. Chem. Phys.* **1995**, *102*, 5917–5936. [CrossRef]

56. Wong, M.W. *Quantum-chemical calculations of sulfur-rich compounds. Elemental Sulfur and Sulfur-Rich compounds II. Topics in Current Chemistry*; Steudel, R., Ed.; Springer: Berlin/Heidelberg, Germany, 2003; Volume 231, pp. 1–29.
57. Swope, W.C.; Lee, Y.-P.; Schaefer, H.F. Diatomic sulfur: Low lying bound molecular electronic states of S_2. *J. Chem. Phys.* **1979**, *70*, 947–953. [CrossRef]
58. Zakrzewski, V.G.; von Niessen, W. Structures, stabilities and adiabatic ionization and electron affinity energies of small sulfur clusters. *Theor. Chim. Acta* **1994**, *88*, 75–96. [CrossRef]
59. Koch, W.; Natterer, J.; Heinemann, C. Quantum chemical study on the equilibrium geometries of S_3 and S_3^-, The electron affinity of S_3 and the low lying electronic states of S_3^-. *J. Chem. Phys.* **1995**, *102*, 6159–6167. [CrossRef]
60. Wong, M.W.; Steudel, R. Structure and spectra of tetrasulfur S_4 − an ab initio MO study. *Chem. Phys. Lett.* **2003**, *379*, 162–169. [CrossRef]
61. Pearson, R.G. *Symmetry Rules for Chemical Reactions: Orbital Topology and Elementary Processes*; John Wiley and Sons: New York, NY, USA, 1976; pp. 78–79.
62. Jones, R.O.; Ballone, P. Density functional and Monte Carlo studies of sulfur. I. Structure and bonding in S_n rings and chains (n = 2–18). *J. Chem. Phys.* **2003**, *118*, 9257–9265. [CrossRef]
63. Chivers, T.; Laidlaw, W.G.; Oakley, R.T.; Trsic, M. Synthesis, crystal and molecular structure of $[(Ph_3P)_2N^+][S_4N^-]$, and the electronic structure of the acyclic anion, S_4N^-. *J. Am. Chem. Soc.* **1980**, *102*, 5773–5781. [CrossRef]
64. Burford, N.; Chivers, T.; Cordes, A.W.; Oakley, R.T.; Pennington, W.T.; Swepston, P.N. Variable geometry of the S_4N^- anion: Crystal and molecular structure of $Ph_4As^+S_4N^-$ and a refinement of the structure of PPN^+ S_4N^- (PPN = $[Ph_3P]_2N^+$). *Inorg. Chem.* **1981**, *20*, 4430–4432. [CrossRef]
65. Donohue, J.; Caron, A.; Goldish, E. The crystal and molecular structure of S_6 (sulfur-6). *J. Am. Chem. Soc.* **1961**, *83*, 3748–3751. [CrossRef]
66. Steudel, R.; Steidel, J.; Pickardt, J.; Schuster, F.; Reinhardt, R. X-ray structural analyses of two allotropes of cycloheptasulfur (γ and δ-S_7). *Z. Naturforsch.* **1980**, *35b*, 1378–1383. [CrossRef]
67. Schmidt, M.; Block, B.; Block, H.H.; Köpf, H.; Wilhelm, E. Cycloheptasulfur, S_7, and cyclododecasulfur, S_{12}: Two new sulfur rings. *Angew. Chem. Int. Ed.* **1968**, *7*, 632–633. [CrossRef]
68. Rettig, S.R.; Trotter, J. Refinement of the structure of orthorhombic sulfur, α-S_8. *Acta Crystallogr.* **1987**, *C43*, 2260–2262. [CrossRef]
69. Bonini, M.G.; Augusto, O. Carbon dioxide stimulates the production of thiyl, sulfinyl, and disulfide radical anion from thiol oxidation by peroxynitrite. *J. Biol. Chem.* **2001**, *276*, 9749–9754. [CrossRef]
70. Yamaji, M.; Tojo, S.; Takehira, K.; Tobita, S.; Fujitsuka, M.; Majima, T. S-S bond mesolysis in α,α′-dinaphthyl disulfide radical anion generated during γ-radiolysis and pulse radiolysis in organic solution. *J. Phys. Chem. A* **2006**, *110*, 13487–13491. [CrossRef]
71. Albright, T.A.; Burdett, J.K.; Whangbo, M.-H. *Orbital Interactions in Chemistry*; John Wiley and Sons: New York, NY, USA, 1985; pp. 212–213.
72. Heilbronner, E.; Bock, H. *The HMO Model and its Application. 1. Basis and Manipulation*; John Wiley and Sons: New York, NY, USA, 1976; pp. 131–132.
73. Chivers, T.; Drummond, I. Characterization of the trisulfur radical anion $S_3^{\bullet-}$ in blue solutions of alkali polysulfides in hexamethylphosphoramide. *Inorg. Chem.* **1972**, *11*, 2525–2527. [CrossRef]
74. Frisch, M.J.; Trucks, G.W.; Schlegel, H.B.; Scuseria, G.E.; Robb, M.A.; Cheeseman, J.R.; Scalmani, G.; Barone, V.; Petersson, G.A.; Nakatsuji, H.; et al. (Eds.) *Gaussian 16*; Revision B.01; Gaussian, Inc.: Wallingford, CT, USA, 2016.
75. Perdew, J.P.; Burke, K.; Ernzerhof, M. Generalized gradient approximation made simple. Generalized gradient approximation made simple. *Phys. Rev. Lett.* **1996**, *77*, 3865–3868. [CrossRef]
76. Berry, D.E.; Fawkes, K.L.; Chivers, T. Student-designed experiment: Preparation and mass spectrum of cyclohexasulfur. *Chem. Educ.* **2001**, *6*, 109–111. [CrossRef]
77. Boeré, R.T.; Chivers, T.; Roemmele, T.L.; Tuononen, H.M. An electrochemical and electronic structure investigation of the $[S_3N_3]^{\cdot}$ radical and kinetic modeling of the $[S_4N_4]_n/[S_3N_3]_n$ (n = 0, −1) interconversion. *Inorg. Chem.* **2009**, *48*, 7294–7306. [CrossRef]
78. Derendorf, J.; Jenne, C.; Keßler, M. The first step of the oxidation of elemental sulfur: Crystal structure of the homopolyatomic sulfur radical cation $[S_8]^{\cdot+}$. *Angew. Chem. Int. Ed.* **2017**, *56*, 8281–8284. [CrossRef]
79. Jagg, P.N.; Kelly, P.F.; Rzepa, H.S.; Williams, D.J.; Woollins, J.D.; Wylie, W. The preparation, x-ray crystal structure and theoretical study of $[CoCp_2][S_3N_3]$, (Cp = cyclopentadienyl), a novel stacking compound incorporating multiple C-H—N(p_π) interactions. *J. Chem. Soc. Chem. Commun.* **1991**, 942–944. [CrossRef]
80. Konchenko, S.N.; Gritsan, N.P.; Lonchakov, A.V.; Irtegova, I.G.; Mews, R.; Ovcharenko, V.I.; Radius, U.; Zibarev, A.V. Cobaltocenium [1,2,5]thiadiazolo[3,4-c][1,2,5]thiadiazolidyl: Synthesis, structure, and magnetic properties. *Eur. J. Inorg. Chem.* **2008**, *2008*, 3833–3838. [CrossRef]
81. Grimme, S.; Antony, J.; Ehrlich, S.; Krieg, H. A consistent and accurate ab initio parametrization of density functional dispersion correction (DFT-D) for the 94 elements H-Pu. *J. Chem. Phys.* **2010**, *132*, 154104. [CrossRef] [PubMed]
82. Chivers, T.; Edelmann, F.; Richardson, J.F.; Schmidt, K.J. A convenient synthesis, X-ray crystal structure and Raman spectrum of the heptasulfide ion, S_7^{2-}, in $[PPN]_2S_7$.2EtOH. *Can. J. Chem.* **1986**, *64*, 145–151. [CrossRef]
83. Adamo, C.; Barone, V.J. Toward reliable density functional methods without adjustable parameters: The PBE0 model. *Chem. Phys.* **1999**, *110*, 6158–6169. [CrossRef]

84. Weigend, F.; Ahlrichs, R. Balanced basis sets of split valence, triple zeta valence and quadruple zeta valence quality for H to Rn: Design and assessment of accuracy. *Phys. Chem. Chem. Phys.* **2005**, *7*, 3297–3305. [CrossRef] [PubMed]
85. Treitel, N.; Shenhar, R.; Aprahamian, I.; Sheradsky, T.; Rabinovitz, M. Calculations of PAH anions: When are diffuse functions necessary? *Phys. Chem. Chem. Phys.* **2004**, *6*, 1113–1121. [CrossRef]
86. Grimme, S. Supramolecular binding thermodynamics by dispersion-corrected density functional theory. *Chem. Eur. J.* **2012**, *18*, 9955–9965. [CrossRef] [PubMed]
87. Grimme, S.; Hansen, A.; Brandenburg, J.G.; Bannwarth, C. Dispersion-corrected mean-field electronic structure methods. *Chem. Rev.* **2016**, *116*, 5105–5154. [CrossRef]
88. Tomasi, J.; Mennucci, B.; Cammi, R. Quantum mechanical continuum solvation models. *Chem. Rev.* **2005**, *105*, 2999–3093. [CrossRef]
89. Wang, C.-W.; Hui, K.; Chai, J.-D. Short- and long-range corrected hybrid density functionals with the D3 dispersion corrections. *J. Chem. Phys.* **2016**, *145*, 204101. [CrossRef]
90. Li, S.L.; Truhlar, D.G. Improving Rydberg excitations within time-dependent density functional theory with generalized gradient approximations: The exchange-enhancement-for-large-gradient scheme. *J. Chem. Theory Comput.* **2015**, *11*, 3123–3130. [CrossRef] [PubMed]
91. Li, Z.; Liu, W. Critical assessment of TD-DFT for excited states of open-shell systems: I. doublet–doublet transitions. *J. Chem. Theory Comput.* **2016**, *12*, 238–260. [CrossRef]
92. Fedunov, R.G.; Pozdnyakov, I.P.; Isaeva, E.A.; Zherin, I.I.; Egorov, N.B.; Glebov, E.M. Sulfur-containing radical anions formed by photolysis of thiosulfate: Quantum-chemical analysis. *J. Phys. Chem. A* **2023**, *127*, 4704–4714. [CrossRef] [PubMed]
93. Chai, J.-D.; Head-Gordon, M. Long-range corrected hybrid density functionals with damped atom–atom dispersion corrections. *Phys. Chem. Chem. Phys.* **2008**, *10*, 6615–6620. [CrossRef]
94. Liang, J.; Feng, X.; Hait, D.; Head-Gordon, M. Revisiting the performance of time-dependent density functional theory for electronic excitations: Assessment of 43 popular and recently developed functionals from rungs one to four. *J. Chem. Theory Comput.* **2022**, *18*, 3460–3473. [CrossRef] [PubMed]
95. *GaussView, Version 6.0.16*; Dennington, R.; Keith, T.A.; Millam, J.M. (Eds.) Semichem Inc.: Shawnee Mission, KS, USA, 2016.